HHS Public Access

Human naïve pluripotent stem cells model X-chromosome dampening and X-inactivation

Anna Sahakyan[1,2], **Rachel Kim**[3], **Constantinos Chronis**[1], **Shan Sabri**[1,3,6], **Giancarlo Bonora**[1,6], **Thorold W. Theunissen**[7], **Edward Kuoy**[1], **Justin Langerman**[1], **Amander T. Clark**[2,3,4,5], **Rudolf Jaenisch**[7,8], and **Kathrin Plath**[1,2,3,4,6,9,*]

[1]Department of Biological Chemistry, University of California, Los Angeles, CA 90095, USA

[2]Molecular Biology Institute, University of California, Los Angeles, CA 90095, USA

[3]Eli and Edythe Broad Center of Regenerative Medicine and Stem Cell Research, University of California, Los Angeles, CA 90095, USA

[4]Jonsson Comprehensive Cancer Center, David Geffen School of Medicine, University of California, Los Angeles, CA 90095, USA

[5]Department of Molecular, Cell and Developmental Biology, University of California, Los Angeles, Los Angeles, CA 90095, USA

[6]Bioinformatics Interdepartmental Program, University of California, Los Angeles, CA 90095, USA

[7]Whitehead Institute for Biomedical Research, Cambridge, MA 02142, USA

[8]Department of Biology, Massachusetts Institute of Technology, Cambridge, MA 02142, USA

Summary

Naïve human embryonic stem cells (hESCs) can be derived from primed hESCs or directly from blastocysts, but their X-chromosome state has remained unresolved. Here, we show that the inactive X-chromosome (X_i) of primed hESCs was reactivated in naïve culture conditions. Like cells of the blastocyst, the resulting naive cells contained two active X-chromosomes with *XIST* expression and chromosome-wide transcriptional dampening, and initiated *XIST*-mediated X-inactivation upon differentiation. Both establishment of and exit from the naïve state (differentiation) happened via an *XIST*-negative X_aX_a intermediate. Together, these findings identify a cell culture system for functionally exploring the two X-chromosome dosage compensation processes in early human development: X-dampening and X-inactivation. However,

*Correspondence: kplath@mednet.ucla.edu (K.P.).
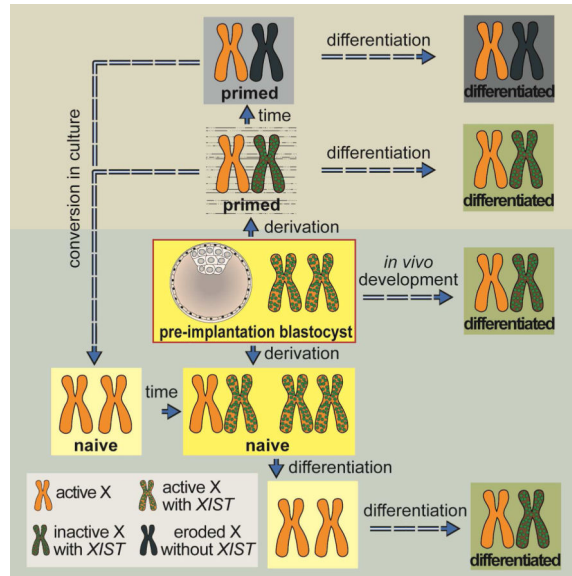[9]Lead Contact

remaining differences between naïve hESCs and embryonic cells related to monoallelic *XIST* expression and non-random X-inactivation highlight the need for further culture improvement. As the naïve state reset X_i abnormalities seen in primed hESCs it may provide cells better suited for downstream applications.

Graphical Abstract

INTRODUCTION

X-chromosome inactivation (XCI) is the silencing of one of the two X-chromosomes in placental female mammals. XCI initiates early in embryonic development during the transition from naïve to primed pluripotency upon implantation of the blastocyst (Minkovsky et al., 2012). Loss- and gain-of-function experiments have demonstrated that the long non-coding RNA *Xist*, itself encoded on the X-chromosome, is the master regulator of XCI. Currently, mechanistic studies of XCI initiation by *Xist* are performed with mouse embryonic stem cells (mESCs) as these cells capture the naïve pluripotent state of epiblast cells of the pre-implantation blastocyst from which they originate. Accordingly, mESCs carry two active X-chromosomes (X_aX_a) that lack *Xist* expression and, upon differentiation, up-regulate *Xist* on one randomly chosen X-chromosome to initiate XCI ($X_aX_i^{Xist+}$, where X_i denotes inactive X-chromosome; Minkovsky et al., 2012). Unlike mESCs, conventional human ESCs (hESCs) do not resemble their embryonic cells of origin, likely as a consequence of culture–induced changes during their derivation. Molecular characteristics such as their post–XCI state (X_aX_i) and resemblance to mouse post–implantation epiblast stem cells classify hESCs as primed pluripotent (Nichols and Smith, 2009). Therefore, studies of XCI initiation in the human system are currently not feasible (Patel et al., in review), and require the establishment of hESCs that recapitulate the pre–XCI state of the pre–implantation embryo.

An additional limitation of female hESCs, as well as human induced pluripotent stem cells (hiPSCs), is the epigenetic instability of the X_i over time in culture, which is characterized by loss of *XIST* RNA and partial transcriptional reactivation, leading to an eroded X_i (X_e; Shen et al., 2008; Silva et al., 2008; Tchieu et al., 2010; Mekhoubad et al., 2012; Nazor et al., 2012). Since loss of *XIST* and X_i-erosion cannot be reversed upon differentiation (Mekhoubad et al., 2012; Nazor et al., 2012; Patel et al., in review), downstream applications of primed female human pluripotent stem cells (hPSCs) are adversely affected by the lack of proper X-chromosome dosage compensation. Hence, hESCs that recapitulate the pre-XCI state of the pre-implantation blastocyst are perhaps better for basic research and therapeutic applications.

Recently, multiple culture conditions have been devised to promote the establishment and maintenance of hPSCs in a naive pluripotent state, either by converting primed hPSCs to the naïve state or by maintaining the naïve state during derivation from the blastocyst (Hanna et al., 2010; Gafni et al., 2013; Chan et al., 2013; Takashima et al., 2014; Ware et al., 2014; Theunissen et al., 2014). To date, the X-chromosome state of naïve hPSCs has remained controversial (Davidson et al., 2015). Molecular characterization of these cells suggests that the diverse culture conditions applied establish pluripotency states of different developmental stages. Notably, two of these protocols (Takashima et al., 2014; Theunissen et al., 2014) achieve a global gene expression profile most similar to cells of human pre-implantation embryos (Huang et al., 2014). These findings raise the possibility that the pre-XCI state of the blastocyst could be captured under these culture conditions.

A distinct characteristic of pluripotent cells of the human — but not mouse — blastocyst is the expression of *XIST* from both active X-chromosomes ($X_a^{XIST+}X_a^{XIST+}$; Okamoto et al., 2011), indicating uncoupling of *XIST* from XCI. In addition, a recent single-cell RNA sequencing study of human pre-implantation embryos described a down-regulation, or dampening, of X-linked genes in female pre-implantation embryos (Petropoulos et al., 2016; Sahakyan and Plath, 2016). Thus, in early human development, an X-chromosome dosage compensation process different from conventional XCI is in play. It is currently unclear if the presence of two active yet *XIST*-expressing X-chromosomes with lowered X-linked gene expression can be captured in cultured female hPSCs.

Here, we studied the X-chromosome state of cells derived by one of the naïve hPSC culture protocols known to closely resemble the pre-implantation state, the 5iLAF-based culture method (Theunissen et al., 2014). 5iLAF media contains small molecule inhibitors targeting MEK, B-Raf, GSK3β, Src, and ROCK, and the growth factors LIF, ActivinA, and FGF2. We discovered that the conversion of primed X_aX_i hPSCs to the naïve state established cells with two active X-chromosomes and expression of *XIST* RNA. The transition to the pre-XCI state was gradual and involved an *XIST*-negative intermediate state with two active X-chromosomes. X-linked genes became down-regulated when cells transitioned from this intermediate to the *XIST*-expressing X_aX_a state, suggesting that dosage compensation of X–linked gene expression by dampening (Petropoulos et al., 2016; Sahakyan and Plath, 2016) occurs in 5iLAF-cultured hPSCs. Naïve hPSCs initiated *XIST*-mediated XCI upon differentiation. These features uniquely resemble the X-chromosome state of the human pre-implantation blastocyst (Okamoto et al., 2011; Petropoulos et al., 2016). Even though the bi-

allelic *XIST* expression pattern of the human blastocyst was consistently captured in naïve hPSCs, the majority of naive cells typically expressed *XIST* from only one of their two active X-chromosomes. Moreover, instead of random XCI, only the prior X_i underwent XCI in differentiating naïve hPSCs, indicating the presence of an epigenetic memory of the primed state in naïve hPSCs, demonstrating the need for further culture modifications. Regardless, we demonstrate that the conversion from primed to naïve pluripotency and subsequent differentiation provide an opportunity to reverse X_i-erosion of primed hPSCs. In summary, our work identifies a cell culture system that enables reversal of X_i erosion and studies of *XIST* function from an active X-chromosome, X-chromosome dampening, and initiation of XCI. Our findings also establish the *XIST*-expressing active X-chromosome as a defining feature of human naïve pluripotency both *in vitro* and *in vivo*.

RESULTS

Primed to naïve conversion leads to X_i-reactivation

We converted the primed female hESC line UCLA1 to naïve pluripotency using the 5iLAF approach (Theunissen et al., 2014). As previously described, 5iLAF media initially resulted in considerable cell death followed by the emergence of dome-shaped colonies that could be passaged as single cells, and induced the up-regulation of key naïve pluripotency markers (Theunissen et al., 2014; Figure S1A and S1B). To examine the expression status of the X-chromosomes, we utilized RNA fluorescent *in situ* hybridization (FISH) to capture sites of nascent transcription at single cell resolution. The primed UCLA1 hESC line used here carried a mostly silent *XIST*-negative X_i with slight erosion due to loss of *XIST* over time in culture (Patel et al., in review). The silencing of the X_i was demonstrated by one nascent transcription spot per nucleus for the X-linked genes *HUWE1, ATRX*, and *THOC2* (Figures 1A–1C) and X_i-erosion by expression of the lncRNA *XACT* (Vallot et al., 2015) from both X-chromosomes (Figure S1C). Since X_i-erosion was very limited in primed UCLA1, we considered this line to be $X_a^{XIST-}X_i^{XIST-}$ in this study.

Upon 19 passages (P19) in 5iLAF media, we detected bi-allelic expression of *HUWE1, ATRX*, and *THOC2* in all cells (Figures 1D–1F), indicating that the transition from primed to naïve pluripotency resulted in X_i-reactivation. Expression of *XACT* remained bi-allelic (Figure S1C) consistent with transcriptional activity of both X-chromosomes. Cells with abnormal X-chromosome count were present in a small proportion of naïve UCLA1 in agreement with previously reported karyotypic abnormalities (Pastor et al., 2016). However, we analyzed only naive cells with two transcription foci of the X-linked gene *UTX*, which escapes XCI (Balaton et al., 2015), to ensure that naïve cells with abnormal X-chromosome count were not included in our quantification.

Naïve hPSCs express *XIST* from an active X-chromosome

At P19 in 5iLAF media, we detected cells with *XIST* expression from both active X-chromosomes (bi-allelic *XIST*, $X_a^{XIST+}X_a^{XIST+}$; Figures 1F and 1G), perfectly recapitulating the blastocyst pattern (Okamoto et al., 2011; Petropoulos et al., 2016). However, the majority of naïve cells displayed *XIST* expression from only one of the two active X-chromosomes (mono-allelic *XIST*, $X_a^{XIST-}X_a^{XIST+}$; Figures 1D–1F). *XIST* RNA

formed a cloud that was often diffuse and appeared more punctate than on a somatic X_i in cells with mono- and bi-allelic *XIST* expression (Figures 1D, 1E, and 1G) reminiscent of the human pre-implantation blastocyst pattern (Okamoto et al., 2011). These findings were reproduced in four independently performed conversions of UCLA1. Together, these results revealed the presence of an *XIST*-expressing X_a in cultured human cells.

Interestingly, naïve pluripotent cells generated from the primed X_aX_i H9 hESC line by inducible expression of NANOG and KLF2 and adaptation to another naïve culture media (t2iL+Gö media, Takashima et al., 2014) also displayed X_i-reactivation (Figure S1D). As in 5iLAF-cultured UCLA1, we observed *XIST* expression from an X_a in t2iL+Gö–adapted H9; however, it was only the mono-allelic (and not bi-allelic) pattern in 3 percent of all cells even after 14 passages post t2iL+Go adaptation ($X_a^{XIST-}X_a^{XIST+}$; Figure S1D). Detection of *XIST* from an X_a by two independent naïve culture approaches further supports the presence of the unique non-silencing *XIST* expression in cultured naïve cells. Since the 5iLAF culture condition induced up-regulation of *XIST* in most cells, we focused our further studies only on naïve hESCs obtained by this method.

Primed to naïve conversion occurs via an *XIST*-negative X_aX_a intermediate

To better understand the dynamics of X_i-reactivation and *XIST* up-regulation in the transition from primed to naïve pluripotency, we analyzed the X-chromosome state during the initial seven passages of UCLA1 in 5iLAF media by RNA FISH for *HUWE1* and *XIST* (Figure 2A). The X_i remained inactive in most cells during the first three passages, but reactivated in all cells by P4. At this time point, *XIST* became induced only in a subset of X_aX_a cells, but continued passaging largely resolved the heterogeneity of *XIST* expression as most cells transitioned to the $X_a^{XIST-}X_a^{XIST+}$ state (Figures 1F and 2A). Bi-allelic *XIST*-expressing cells were generally detected together with mono-allelic ones, but did not increase in numbers over time (Figures 1F and 2A). These results indicated that cells gradually change their X-chromosome state in 5iLAF media, progressing from the X_aX_i state to the *XIST*-expressing end-state with two active X-chromosomes via an *XIST*-negative X_aX_a intermediate. Consistent with this, we found that *XIST*-negative X_aX_a cells obtained by sub-cloning of an early passage heterogeneous naïve UCLA1 culture (clone 4) converted to the $X_a^{XIST-}X_a^{XIST+}$ / $X_a^{XIST+}X_a^{XIST+}$ state with passaging, where again the bi-allelic *XIST* expressing cells were a minority (Figure S1E and S1F). Conversely, naïve *XIST*-positive X_aX_a sub-clones (clones 9 and 12) did not change their *XIST*-expression status and stably maintained their predominantly mono-allelic and some bi-allelic *XIST* expression over time. The *XIST*-negative X_aX_a intermediate was also observed when primed hiPSCs carrying an *XIST*-positive X_i (prior to *XIST* loss and X_i-erosion) were converted to naïve pluripotency, indicating that the presence of *XIST* in the primed state did not interfere with the sequence of events leading to X_i-reactivation (Figure S1G). Thus, the transition from the *XIST*-expressing X_i to the *XIST*-expressing X_a involves silencing and re-expression of *XIST* (see Table S1 for a summary of X-chromosome states of hPSCs used in this study).

X$_i$-reactivation in naïve hESCs is chromosome-wide

To address whether X$_i$-reactivation happened chromosome-wide, we assessed the expression of multiple X-linked genes in an allele-specific manner based on single nucleotide polymorphisms (SNPs). We applied either Sanger sequencing of RT-PCR products or RNA sequencing (RNA-seq) to measure the proportion of transcripts containing the reference and alternate SNP for a given X-linked gene. In primed UCLA1, almost all tested X-linked genes normally subject to XCI expressed only one of the two alleles, i.e. either solely the reference or the alternate allele (Figures 2B, S2A, and S2E), demonstrating that the same X-chromosome was inactive in all cells. This finding was not surprising because hESC lines tend to be clonal (Shen et al., 2008). Only one gene normally subject to XCI displayed expression of both alleles (*TCEAL4*, SNP rs11010) similar to genes known to escape XCI (Figures 2B and S2A) likely due to the slight X$_i$ erosion in primed UCLA1.

The non-random XCI state of primed UCLA1 line allowed us to determine at the population level whether the entire X$_i$ reactivated in the naïve state, which would lead to the expression of both alleles. We defined the allelic expression pattern in our three X$_a$X$_a$ sub-clones of naïve UCLA1: clone 4 at early passage when it was largely *XIST*-negative and the *XIST*-positive clones 9 and 12. Our analysis showed that all X-linked genes with mono-allelic expression in primed UCLA1 were bi-allelically expressed in the naive clones (Figures 2B and S2B–S2E). These findings were corroborated by RNA-seq at the single cell level (Figure 2C). In *XIST*-negative and *XIST*-positive single cells of naïve UCLA1 (at early and late passage post 5iLAF adaptation, respectively), single cell RNA-seq detected reads from both X-chromosomes for genes that had only the reference or the alternate allele expressed in the starting primed cells (Figure 2C). These data demonstrated the reactivation of a larger number of X-linked genes, distributed across the entire X-chromosome, in both the *XIST*-negative and *XIST*-positive naïve hESCs, supporting and extending our RNA FISH-based conclusion of X$_i$-reactivation.

The single cell RNA-seq analysis also allowed us to examine the allelic origin of *XIST* expression in naïve UCLA1. The majority of the *XIST*-positive X$_a$X$_a$ cells (26 of 46, 57%) expressed only the alternate allele of *XIST* (based on SNP rs1620574), which was corroborated by Sanger sequencing of the *XIST* RT-PCR product at the population level (Figure S2F). This allele was expressed from the X$_i$ in early passage primed UCLA1. However, 28% of single naïve cells (13 of 46) expressed both alleles of *XIST*, perfectly recapitulating the blastocyst pattern (Figure S2F). We had estimated this to be closer to 5% by RNA FISH (Figures 1 and 2A) most likely due to lower sensitivity of RNA FISH compared to single cell RNA-seq. Interestingly, 15% of cells (7 of 46) expressed only the *XIST* carrying the reference allele of SNP rs1620574 (Figure S2F), indicating that either of the two X-chromosomes has the ability to up-regulate *XIST* in naïve cells.

X–inactivation specific de-methylation occurs faster than global hypo-methylation in the primed to naïve transition

DNA methylation of CpG islands (CGIs) is a key characteristic of XCI (Sharp et al., 2011). We utilized reduced representation bisulfite sequencing (RRBS; Meissner, 2005) to examine methylation levels in primed UCLA1 and the naïve clones 4, 9 and 12 as expression-

independent evidence of X_i-reactivation. The intermediary methylation typical for X_i-linked CGIs was observed in primed UCLA1, but largely absent in the naïve clones where it was reduced to the level of a male control (X_aY, primed UCLA10 hESC line) consistent with chromosome-wide X_i-reactivation in naïve cells with and without *XIST* expression (Figure 2D).

CpGs outside of CGIs are not subject to regulation by XCI (Sharp et al., 2011). Notably, the naïve clones displayed significant de-methylation of X-linked and autosomal CpGs outside the context of CGIs, consistent with reaching the globally hypo-methylated state of the human pre-implantation epiblast (Smith et al., 2014; Pastor et al., 2016; Theunissen et al., 2016; Figures 2E, S3A and S3B). However, in this context, the *XIST*-negative X_aX_a clone 4 was not as dramatically de-methylated as the *XIST*-expressing clones 9 and 12 (Figures 2E, S3A, and S3B). This was also true for imprint control regions where hypo-methylation was detectable in the naïve state but was much less prominent in clone 4 than clones 9 and 12 (Figure S3C), suggesting that global de-methylation and imprint de-methylation occurred more slowly than X-linked CGI de-methylation associated with X_i-reactivation. Indeed, the quantification of average methylation levels demonstrated that the methylation loss within X-linked CGIs of clone4 was far more significant compared to non-CGI CpGs both in chromosome X and autosomal context (Figures 2F and S3D). Together, these results hint at the presence of an active de-methylation process of CGIs on the X_i in the transition from primed to naïve pluripotency. The X-specific nature of this process was further highlighted by the fact that autosomal CGIs became de-methylated at the global hypo-methylation rate of non-CGIs (Figures 2F, S3A and S3D).

Transition from the *XIST*-negative to the *XIST*-positive naïve state is accompanied by dampening of X-linked gene expression

Given the changes of *XIST* expression and DNA methylation from primed to early- and late-passage naïve hESCs, we asked whether gene expression also changed with this progression (Figure S3E). We compiled lists of genes known to be up- or down-regulated in naïve versus primed pluripotent cells based on single cell RNA-seq data of epiblast cells of human blastocysts and primed hESCs (Yan et al., 2013; Table S2). We found that the naïve clone 4 at early passage, when it was still *XIST*-negative, exhibited an incomplete down-regulation of genes that have higher expression in primed than naïve state (Figure S3F). However, on average, it achieved up-regulation of naïve-specific genes as efficiently as the *XIST*-positive naïve clones 9 and 12 (Figure S3G). The incomplete hypo-methylation as well as down-regulation of primed-specific genes in clone 4 supported the classification of the *XIST*-negative X_aX_a state as an intermediate in the transition from primed to naïve pluripotency.

Although both *XIST*-positive and -negative naïve clones harbored two active X-chromosomes, we found that the *XIST*-negative clone4 exhibited significantly higher X-linked, but not autosomal, gene-expression compared to the *XIST*-positive clones 9 and 12 (Figure 2G). Importantly, upon transition to the *XIST*-positive state, clone4 specifically reduced the expression of genes on the X-chromosome, but not autosomes (Figure 2G), indicating that this difference could not be simply explained by clonal differences. This was also the case for an early, *XIST*-negative passage of naïve cells derived from a different

primed female hESC line, UCLA4, compared to late passage *XIST*-positive cells of the same line (Figure 2H). Thus, the decrease of X-linked transcript levels consistently occurred during the transition from the *XIST*-negative to the *XIST*-positive naïve X_aX_a state.

The lowered expression of X-linked genes in *XIST*-positive naïve cells mirrored the dampened X-linked gene expression recently described in female human pre-implantation embryos, where X-chromosome dampening (XCD) also coincided with up-regulation of *XIST* during pre-implantation development (Petropoulos et al., 2016). The comparison of *XIST*-expressing X_aX_a UCLA1 naïve clones to the starting X_aX_i primed UCLA1 cells revealed similar extent of X-linked gene expression in both, even though the former had two active X-chromosomes and the latter only one (Figure S3H).

H3K27me3 accumulates on the *XIST*-expressing X_a in naïve cells

A common feature of the *XIST*-expressing X_i is the accumulation of the repressive histone modification H3K27me3 and exclusion of RNA polymerase II in immunofluorescence experiments (Plath et al., 2003). To understand the function of *XIST* on the X_a further, we examined the distribution of H3K27me3 by immunostaining coupled to *XIST* RNA FISH in naïve UCLA1 clone12 cells and in normal female $X_aX_i^{XIST+}$ fibroblasts as control. We detected an enrichment of H3K27me3 on the *XIST*-expressing X_a similar to fibroblasts (Figure 3A). Notably, H3K27me3 enrichment is not sufficient for silencing the X-chromosome in mouse (Plath et al., 2003) consistent with the notion that the accumulation of this mark can occur on an active X. In agreement with the *XIST*-expressing X-chromosome being active, we failed to detect clear exclusion of RNA polymerase II from the *XIST*-expressing X_a in naïve UCLA1 clone 12, whereas the exclusion was very obvious in normal female fibroblasts (Figure 3B).

Blastocyst-derived naïve hESCs capture the *XIST*-positive but not the *XIST*-negative X_aX_a state

For late passage naïve cells obtained from UCLA1 and hiPSCs, the majority of cells expressed *XIST* from one active X-chromosome and X_aX_a cells expressing *XIST* bi-allelically were consistently a minority (Figures 1, 2A, and S1G). This result was also obtained for all other primed to naïve cell line conversions performed in this study (Table S1). In addition, we confirmed that the originally described naïve WIBR3 hESC line (Theunissen et al., 2014) showed reactivation of the X_i and induction of *XIST* from one X_a and more seldom from both X-chromosomes (Figures 3C and S4). These proportions did not change when primed hESCs were converted to naïve pluripotency without FGF2 (5iLA) or without the GSK3β inhibitor IM-12 and FGF2 (4iLA; Figures 3C and S4; Theunissen et al., 2016). Elimination of other inhibitors of the 5iLAF media interfered with cell growth and/or morphology.

An intriguing question was what the X-chromosome state would be like in naïve cells derived directly from pre-implantation blastocysts in 5iLAF media. We found that the $X_a^{XIST-}X_a^{XIST+}$ pattern was also dominant in two female naïve hESC lines, UCLA19n and UCLA20n, which we directly derived from human blastocysts (Pastor et al., 2016). Interestingly, the proportion of cells expressing *XIST* bi-allelically was raised to nearly 40%

at the expense of mono-allelic *XIST*-expressing cells (Figure 3D). Another interesting observation was that *XIST*-negative X_aX_a cells were largely lacking in embryo-derived lines even at early passage (Figure 3D). We conclude that the 5iLAF culture condition supports the *XIST*-positive X_aX_a state regardless of cell origin, that the transient *XIST*-negative X_aX_a state is unique to the primed to naïve transition, and that naïve $X_a^{XIST+}X_a^{XIST+}$ cells are stabilized more effectively when naïve hESCs are derived directly from the embryo. Similar to naïve cells derived from primed hESCs, blastocyst-derived naïve cells displayed H3K27me3 accumulation and lacked exclusion of RNA polymerase II on the *XIST*-coated X_a (Figures 3A and 3B).

Naïve hESCs induce XCI upon differentiation

Next, we asked whether naïve hESCs were capable of undergoing XCI upon differentiation. Direct differentiation from the 5iLAF condition resulted in extensive cell death; hence, we re-adapted the naive cells to the primed culture condition (called re-primed state) before inducing differentiation. When starting from naïve $X_a^{XIST-}X_a^{XIST+}$ UCLA1, *XIST* expression was lost in the re-primed state while both X-chromosomes remained active and displayed a higher dose of gene expression (Figures 4A and Figure S3I). Upon differentiation of re-primed cells, one of the two X-chromosomes up-regulated *XIST* in around 80% of cells and the majority of cells with an *XIST* RNA cloud displayed silencing as measured by RNA FISH for the X-linked gene *HUWE1* (Figures 4A and 4B). The *XIST*-coated X-chromosome was still actively expressing *HUWE1* in a fraction of differentiated cells, but the nascent *HUWE1* transcription focus was smaller compared to that on the *XIST*-negative X-chromosome (Figure 4B), suggesting that XCI was initiated but not completed. Re-priming and differentiation of the blastocyst-derived naïve hESC line UCLA20n also resulted in loss of *XIST* in the re-primed state followed by *XIST*-mediated XCI upon differentiation (Figure 4C). Thus, we describe a pre-XCI state in cultured hPSCs that can faithfully induce *XIST*-mediated XCI. Additionally, the data suggest that the developmental path from the *XIST*-positive X_aX_a naïve state to XCI occurs by first down-regulating *XIST* on the X_a and then inducing it again on the future X_i, reverting the sequence of events that took place in establishing naïve pluripotent cells from the primed state.

XCI in differentiating naïve hPSCs is non-random

To address whether XCI occurred randomly on one of the two X-chromosomes, as normally observed in development, we analyzed the allelic expression of X-linked genes in single cells after seven days of differentiation from the re-primed state of UCLA1. We found that almost all individual differentiated cells expressed only one allele of *XIST* and of the X-linked genes normally subject to XCI (Figures 5A–5C). For *XIST* as well as the X-linked genes (with one exception), it was the allele previously expressed in the starting primed cells. Genes escaping XCI expressed both alleles in the primed, naïve, and differentiated states, validating the robustness of our assays (Figures S2, S5A, and S5B). These data demonstrated that XCI in differentiating naïve hESCs is non-random, suggesting the presence of an epigenetic memory of the X_i inherited from the primed state.

Next, we tested if non-random XCI also is a feature of differentiating naïve cells that were derived from a population of cells known to undergo random XCI. We generated primed hiPSC lines from Rett syndrome patient fibroblasts harboring a heterozygous mutation in the X-linked gene *MECP2* that leads to the absence of the MeCP2 protein product (Lee et al., 2001). Consequently, the presence of the MeCP2 protein indicated that the wild type allele was on the X_a, while lack of MeCP2 indicated that the mutant allele was on the X_a. In resulting hiPSC lines, all cells either expressed the MeCP2 protein (clone 16, $X_a^{MECP2\,wt}$ $X_i^{MECP2\,mut}$) or did not (clone 17, $X_a^{MECP2\,mut}$ $X_i^{MECP2\,wt}$) (Figures 5D and S5C), consistent with the clonal nature of hiPSCs with respect to XCI-status (Tchieu et al., 2010). Due to its MeCP2-negative starting state, clone 17 was most informative for our analysis. X_i-reactivation was captured with the detection of the MeCP2 protein in most cells of clone 17 at early passage in 5iLAF media (P3; Figure S5C) and was maintained in the re-primed state (Figure 5D). Subsequent differentiation, confirmed by expression of the negative pluripotency cell-surface marker CD44, induced complete loss of MeCP2 in clone 17 — and not mosaic MeCP2 expression which would be expected for random XCI — reverting back to the original state where the X-chromosome bearing the wild-type *MECP2* allele was inactivated ($X_a^{MECP2mut}$ $X_i^{MECP2wt}$; Figures 5D and S5D). As observed in UCLA1, silencing of the X-chromosome in differentiated cells correlated with *XIST* up-regulation (Figure S5E). For clone16, all cells maintained MeCP2 expression in the naïve, re-primed, and differentiated states (Figures 5D and S5C–S5E). We conclude that naïve clones obtained from a population of randomly inactivated cells underwent non-random XCI upon differentiation and that the epigenetic memory for the X_i was maintained in naïve hESCs as well as in hiPSCs (Figure 5E). Future experiments will demonstrate whether the X_i memory is due to residual DNA methylation or histone modifications that persist in the naïve and re-primed states, or perhaps involves other mechanisms.

X_i abnormalities of primed hESCs are erased in the naïve state

We tested whether the naïve state would correct the epigenetic abnormalities of the X_i prevalent in female primed hPSCs. *XIST* typically becomes silenced in primed hPSCs over time in culture, which is often associated with X_i erosion (Shen et al., 2008; Silva et al., 2008; Tchieu et al., 2010; Mekhoubad et al., 2012; Nazor et al., 2012; Vallot et al., 2015; Patel et al., 2017). Importantly, the X-chromosome state does not change upon differentiation of eroded (X_aX_e) primed hPSCs, giving rise to differentiated daughter cells with improper X-chromosome dosage compensation. Primed hESC lines can also be in an extremely aberrant X_aX_a state that cannot undergo XCI upon differentiation (Patel et al., 2017). Currently, methods are lacking to overcome these epigenetic abnormalities of the X-chromosome in primed hPSCs and their differentiated daughter cells. Since our experiments with UCLA1 demonstrated that *XIST*-mediated XCI was present in differentiated cells only after transition through the naïve state, but never when starting from primed cells (Patel et al., 2017); Figures 4A, 4B, 5A–5C and S6A), we decided to examine the X-chromosome state in hESC lines with extreme epigenetic abnormalities of the X.

In the primed state, the hESC line UCLA9 carried two active X-chromosomes without *XIST* expression and did not display any evidence of XCI upon differentiation from the primed state, as shown by RNA FISH for the X-linked genes *HUWE1*, *ATRX*, and *THOC2* (Patel et

al., in review; Figures 6A, 6B and S6B–S6D). Upon adaptation to the 5iLAF condition, the X-linked genes remained bi-allelically expressed and *XIST* was gradually induced (Figure 6C). Similar to UCLA1, at later passage, the majority of naïve UCLA9 cells expressed *XIST* mono-allelically albeit some bi-allelic *XIST*-expressing cells were consistently detected (Figure 6C and 6D). Upon transition to the re-primed state, *XIST* was silenced again and bi-allelic expression of X-linked genes was maintained (Figures 6D and 6E). Importantly, differentiation from the re-primed state induced XCI with *XIST* expression shown by silencing of *HUWE1*, *ATRX* and *THOC2* (Figures 6D, 6F, S6E and S6F). Thus, the naïve state allowed the differentiation product of starting primed cells with abnormal X_aX_a state to have a proper X_i with *XIST* expression (Figure 6G).

We extended this analysis to the hESC line UCLA4. Primed UCLA4 and its differentiated daughter cells carried an *XIST*-negative X_e (Patel et al, in review). We captured the X_aX_e state by the differential expression of the X-linked genes *HUWE1* and *ATRX* (Figures 7A and S7A–S7C). Specifically, *HUWE1*, which was not affected by X_i erosion, was mono-allelically expressed in primed UCLA4 and its differentiated product. Conversely, *ATRX* had bi-allelic expression in primed UCLA4 due to X_i-erosion and retained this expression pattern upon differentiation from the primed state. *HUWE1* became bi-allelically expressed in the naive states consistent with reactivation of the X_e, while *ATRX* retained its bi-allelic expression (Figures 7B and 7C). The transition to the naïve state was accompanied by *XIST* induction mostly in its mono-allelic form, albeit some bi-allelic cells were again observed (Figures 7B and 7C). We confirmed that at P9 naïve UCLA4 hESCs were largely karyotypically normal (Figure S7D). Re-priming was associated with the maintenance of bi-allelic X-linked gene expression and loss of *XIST* (Figures 7C and 7D). Upon differentiation from the re-primed state, both *HUWE1* and *ATRX* were silenced on one X-chromosome and *XIST* was expressed from the X_i (Figures 7C–7E). Together, these data demonstrate the ability of differentiating naïve cells to undergo XCI even when derived from primed X_aX_a and X_aX_e hESCs (Figures 6G and 7F).

DISCUSSION

A key difference between mouse and human development is the X-chromosome state of the female pre-implantation embryo. In the mouse, the paternally– inherited X-chromosome becomes silenced at the 4–8 cell stage due to imprinted XCI. At the blastocyst stage, the imprinted X_i is reactivated specifically in epiblast cells to allow random XCI in embryonic cells upon implantation (Minkovsky et al., 2012). Intriguingly, imprinted XCI does not occur in human pre-implantation embryos (Petropoulos et al., 2016). Another distinguishing feature between mouse and human is that epiblast cells of the mouse blastocyst harbor two active X-chromosomes that do not express *Xist*, whereas in human pre-implantation embryos both active X-chromosomes are marked by *XIST* expression (Okamoto et al., 2011). Since naïve hPSCs of the mouse resemble the X-chromosome state of the epiblast cells of the *mouse* blastocyst, in our study we addressed whether human naïve hPSCs can capture the unique X-chromosome state of the *human* blastocyst. We applied independent approaches such as RNA FISH and SNP-based allelic expression profiling by single cell RNA-sequencing to robustly assess the X-chromosome state in naïve hPSCs at single cell

resolution, as well as bulk RNA-sequencing and DNA methylation analyses at the cell population level.

Our data demonstrate that the naïve 5iLAF culture condition captures an X-chromosome state resembling that of the human blastocyst (Okamoto et al., 2011; Petropoulos et al., 2016). Specifically, we found that 5iLAF-cultured female naïve cells carry two active X-chromosomes, express *XIST* from the active X-chromosome(s), display dampening of X-linked gene expression, and undergo *de novo* X-inactivation upon differentiation. These results were robust and highly reproducible, regardless of whether naïve hPSCs were derived directly from the blastocyst or primed hESCs or hiPSCs, or established in different laboratories (Plath and Jaenisch). Also, our results are entirely consistent with data published recently (Theunissen et al, 2016). Therefore, our work identifies a cell culture system for the mechanistic study of the unique and human-specific form of X-chromosome dosage compensation that results in dampening, but not silencing, of X-linked gene expression early in human development, and for the function of *XIST* on an active X-chromosome. Moreover, our findings enable the molecular dissection of the transition from XCD to XCI and of the mechanisms of XCI initiation in human embryonic development. Most of our current understanding of how *XIST* initiates XCI comes from studies in mouse ESCs, but it is yet to be seen if human *XIST* functions similarly to its mouse homologue in XCI initiation. In addition, our findings clarify the question of the X-chromosome pattern in naïve hPSCs, which has remained controversial (Davidson et al., 2015).

Despite the similarities of the X-chromosome state in 5iLAF-cultured naïve hPSCs and cells of the blastocyst, we found several key differences. First, the mono-allelic *XIST*-expressing X_aX_a state was predominant in naïve hPSCs. The $X_a^{XIST+}X_a^{XIST+}$ pattern, perfectly recapitulating that of the blastocyst, was consistently observed yet only in a subset of cells. Second, the observation of non-random XCI upon differentiation from the naïve state does not reflect the randomness of the process normally seen in development. Moreover, the fact that it is the same inactive X-chromosome of the starting primed hESCs that becomes inactivated in differentiated naïve cells indicates the existence of an epigenetic memory for the prior X_i that does not get erased in the naïve state. Third, we observed an accumulation of the repressive H3K27me3 histone modification on the *XIST*-coated X_a that has not been described for the blastocyst (Okamoto et al., 2011). However, it is unclear whether the lack of H3K27me3 accumulation on the X in cells of the blastocyst is due to differential staining of cultured cells and embryos, or a reflection of a different X-chromosome state. Regardless, together these findings indicate that additional modifications to the naïve culture media are required to reset these features to the most faithful state. However, it is noteworthy that naïve hESCs directly derived from the blastocyst in 5iLAF media had higher proportion of $X_a^{XIST+}X_a^{XIST+}$ cells. Additionally, our data suggest that the non-randomness of XCI and the memory of the prior X_i from the primed state in differentiating naïve cells are not linked to the mono-allelic expression status of *XIST* in the naïve state. Single cell and population analyses revealed that either of the two X-chromosomes is capable of up-regulating *XIST* in naïve cells (Figure S2F), yet upon differentiation there is very heavy skewing towards inactivating the prior X_i, resulting in non-random XCI. Moreover, *XIST* expression is silenced in the transition from primed to naïve and prior to differentiation in the re-primed state, arguing against *XIST*'s direct involvement in X_i memory.

X_i-reactivation was not limited to the 5iLAF culture condition. Interestingly, we found that the t2iL+Gö culture media (Takashima et al., 2014) also induced X_i-reactivation in primed hPSCs in all cells and mono-allelic *XIST* expression from an active X-chromosome in a subset of cells. This result is in agreement with global gene expression studies that have placed naïve cells generated by the 5iLAF and t2iL+Gö conditions closest to the blastocyst state (Huang et al., 2014). The detection of the *XIST*-expressing X_a in two independent naïve culture conditions establishes the *XIST*-expressing active X-chromosome as a hallmark of human naïve pluripotency in cultured cells. The X_a^{XIST+} provides a straightforward readout for characterizing the constantly evolving naïve media formulations, which will immensely help in improving naïve culture conditions. Interestingly, we found that in t2iL+Gö condition (Takashima et al., 2014) most cells did not express *XIST* despite harboring two active X-chromosomes, consistent with the notion that the different media compositions for naïve cells may capture pluripotent states at slightly different stages of development (Huang et al., 2014).

Another interesting outcome of our work is the finding that the transition from an *XIST*-expressing X_a in the naïve state to the *XIST*-expressing X_i in differentiated cells occurs through an intermediate in which both X-chromosomes are actively expressed but *XIST* is off. Although both *XIST*-negative and -positive naïve cells had the ability to undergo *de novo* XCI upon differentiation, gene expression and DNA methylation analysis indicated *XIST* expression from an active X-chromosome as a more stringent marker of the blastocyst-like naïve pluripotent state than the presence of two active X-chromosomes alone. The *XIST*-negative X_aX_a intermediate was also observed during X_i-reactivation in the reverse process during the transition from primed X_aX_i hPSCs to naïve *XIST*-expressing X_aX_a cells. Hence, we speculate that in the developing human embryo *XIST* expression turns off during the transition from XCD to XCI. Intriguingly, during derivation of primed hESC from blastocysts, we found that cells rapidly lost *XIST* expression from both active X-chromosomes, yielding a mixture of X_aX_a cells without *XIST* and $X_a^{XIST-}X_i^{XIST+}$ cells where *XIST* is expressed from the X_i in a post-XCI manner (Patel et al, in review). This further supports our classification of the *XIST*-negative X_aX_a cells as a developmental intermediate in the transition from pre- to post-XCI.

In both the primed to naïve transition *in vitro* and human pre-implantation development, the dampening of X-linked gene expression correlated with up-regulation of *XIST*, suggesting that this unique form of X-chromosome dosage compensation may be *XIST*-dependent. If this was the case, dampening should only affect one X-chromosome in naïve hPSCs with mono-allelic *XIST* and both X-chromosomes in cells with bi-allelic *XIST*. Understanding this requires in-depth examination of X-linked allele-specific gene expression patterns at the single cell level so that the expression of the *XIST*-expressing X can be compared to that of the *XIST*-negative one in the same cell. Such analyses require multiple cells with deeply sequenced high-quality data for meaningful conclusions, and unfortunately our single-cell analyses were not sufficient for resolving this question. The dampened expression of X-linked genes in naïve hPSCs may explain why originally described naïve female hESCs were thought to harbor an X_i based on global gene expression analysis (Theunissen et al., 2014). Hence, methods beyond global gene expression changes should be used to assess the X-chromosome status of hESCs.

Lastly, our findings demonstrated that the exposure to the naïve state reverses the epigenetic abnormalities of the X_i prevalent in female primed hiPSC and hESC lines, including loss of *XIST*, X_i-erosion and the inability to induce X-inactivation upon differentiation. Since erroneous X-chromosome dosage compensation has been linked to developmental abnormalities and cancer in both mouse and human (Schulz and Heard, 2013), this result is critical for the application of female hPSCs as it enables the generation of differentiated cells with properly dosage-compensated X-chromosomes. One concern is that imprint methylation erasure and karyotypic abnormalities are observed in the 5iLAF-based naïve culture condition. We observed faithful XCI in hPSCs that were kept in the naïve condition for only few passages and these cells remain karyotypically normal and maintain methylation at imprint control regions (Theunissen et al., 2014; Pastor et al., 2016; Figure S3C). Hence, our work suggests a path towards hPSCs without undesirable genetic and epigenetic abnormalities, which is more desirable for cell replacement therapies and more apt for studies of basic development and diseases.

EXPERIMENTAL PROCEDURES

Cell Culture

Primed hPSCs were cultured on feeder cells and passaged with collagenase IV every 6–7 days. Primed hPSCs were converted to 5iLAF naïve condition as described (Theunissen et al., 2014). Briefly, 2×10^5 primed single cells were plated on feeders in primed media with ROCK inhibitor Y-27632 for two days before switching to 5iLAF. Ten days later, surviving cells were passaged as single cells. For re-priming, 5iLAF media was changed to primed when naïve colonies were of medium size and thereafter cells were treated exactly as primed cultures. For differentiation, primed or re-primed hPSC cultures were depleted of feeder cells and plated as single cells on matrigel–coated plates or coverslips for 7 days in fibroblast media (see Supplemental Experimental Procedures for more details).

RNA FISH and Microscopy

Cells grown on gelatinized glass coverslips were fixed with 4% formaldehyde, permeabilized with 0.5% Triton X-100 (10 min each), and serially dehydrated with 70–100% ethanol. Coverslips were hybridized with labeled DNA probes generated from BACs. The Imager M1 microscope (Zeiss) was used for acquiring and ImageJ software (NIH) for processing z-stack images (see Supplemental Experimental Procedures for more details).

RNA-sequencing

RNA-seq libraries were prepared using the TruSeq Stranded mRNA Library Prep Kit (Illumina). The C_1 Single-Cell Auto Prep System (Fluidigm) was used for single cell RNA-seq. Allelic expression proportions were determined either by read counts (RNA-seq) or Sanger sequencing of exonic SNPs of X-linked genes (see Supplemental Experimental Procedures for more details).

DNA methylation

Genomic DNA was harvested from replicate samples and libraries for Reduced Representation Bisulfite Sequencing (RRBS) were created as previously described

(Meissner, 2005). Only CpG sites covered by at least five reads across all samples under consideration were used for data presentation (see Supplemental Experimental Procedures for more details).

Data deposition

RNA-seq and RRBS data have been deposited at the GEO database (www.ncbi.nlm.nih.gov/geo/) with the accession number GSE87239.

Supplementary Material

Refer to Web version on PubMed Central for supplementary material.

Acknowledgments

REFERENCES

Balaton BP, Cotton AM, Brown CJ. Derivation of consensus inactivation status for X-linked genes from genome-wide studies. Biol. Sex Differ. 2015; 6:35. [PubMed: 26719789]

Chan Y-S, Göke J, Ng J-H, Lu X, Gonzales KAU, Tan C-P, Tng W-Q, Hong Z-Z, Lim Y-S, Ng H-H. Induction of a Human Pluripotent State with Distinct Regulatory Circuitry that Resembles Preimplantation Epiblast. Cell Stem Cell. 2013; 13:663–675. [PubMed: 24315441]

Davidson KC, Mason EA, Pera MF. The pluripotent state in mouse and human. Development. 2015; 142:3090–3099. [PubMed: 26395138]

Gafni O, Weinberger L, Mansour AA, Manor YS, Chomsky E, Ben-Yosef D, Kalma Y, Viukov S, Maza I, Zviran A, et al. Derivation of novel human ground state naive pluripotent stem cells. Nature. 2013; 504:282–286. [PubMed: 24172903]

Hanna J, Cheng AW, Saha K, Kim J, Lengner CJ, Soldner F, Cassady JP, Muffat J, Carey BW, Jaenisch R. Human embryonic stem cells with biological and epigenetic characteristics similar to those of mouse ESCs. Proc. Natl. Acad. Sci. 2010; 107:9222–9227. [PubMed: 20442331]

Huang K, Maruyama T, Fan G. The Naive State of Human Pluripotent Stem Cells: A Synthesis of Stem Cell and Preimplantation Embryo Transcriptome Analyses. Cell Stem Cell. 2014; 15:410–415. [PubMed: 25280217]

Lee SS, Wan M, Francke U. Spectrum of MECP2 mutations in Rett syndrome. Brain Dev. 2001; 23(Suppl 1):S138–S143. [PubMed: 11738860]

Meissner A. Reduced representation bisulfite sequencing for comparative high-resolution DNA methylation analysis. Nucleic Acids Res. 2005; 33:5868–5877. [PubMed: 16224102]

Mekhoubad S, Bock C, de Boer AS, Kiskinis E, Meissner A, Eggan K. Erosion of Dosage Compensation Impacts Human iPSC Disease Modeling. Cell Stem Cell. 2012; 10:595–609. [PubMed: 22560080]

Minkovsky A, Patel S, Plath K. Concise Review: Pluripotency and the Transcriptional Inactivation of the Female Mammalian X Chromosome. STEM CELLS. 2012; 30:48–54. [PubMed: 21997775]

Nazor KL, Altun G, Lynch C, Tran H, Harness JV, Slavin I, Garitaonandia I, Müller F-J, Wang Y-C, Boscolo FS, et al. Recurrent Variations in DNA Methylation in Human Pluripotent Stem Cells and Their Differentiated Derivatives. Cell Stem Cell. 2012; 10:620–634. [PubMed: 22560082]

Nichols J, Smith A. Naive and Primed Pluripotent States. Cell Stem Cell. 2009; 4:487–492. [PubMed: 19497275]

Okamoto I, Patrat C, Thépot D, Peynot N, Fauque P, Daniel N, Diabangouaya P, Wolf J-P, Renard J-P, Duranthon V, et al. Eutherian mammals use diverse strategies to initiate X-chromosome inactivation during development. Nature. 2011; 472:370–374. [PubMed: 21471966]

Pastor WA, Chen D, Liu W, Kim R, Sahakyan A, Lukianchikov A, Plath K, Jacobsen SE, Clark AT. Naive Human Pluripotent Cells Feature a Methylation Landscape Devoid of Blastocyst or Germline Memory. Cell Stem Cell. 2016; 18:323–329. [PubMed: 26853856]

Patel, et al. We will add in the related Cell Reports paper here. 2017

Petropoulos S, Edsgärd D, Reinius B, Deng Q, Panula SP, Codeluppi S, Plaza Reyes A, Linnarsson S, Sandberg R, Lanner F. Single-Cell RNA-Seq Reveals Lineage and X Chromosome Dynamics in Human Preimplantation Embryos. Cell. 2016

Plath K, Zhang Y, Panning B, Otte AP. Role of Histone H3 Lysine 27 Methylation in X Inactivation. Science. 2003; 300:131–135. [PubMed: 12649488]

Sahakyan A, Plath K. Transcriptome Encyclopedia of Early Human Development. Cell. 2016; 165:777–779. [PubMed: 27153491]

Schulz EG, Heard E. Role and control of X chromosome dosage in mammalian development. Curr. Opin. Genet. Dev. 2013; 23:109–115. [PubMed: 23465885]

Sharp AJ, Stathaki E, Migliavacca E, Brahmachary M, Montgomery SB, Dupre Y, Antonarakis SE. DNA methylation profiles of human active and inactive X chromosomes. Genome Res. 2011; 21:1592–1600. [PubMed: 21862626]

Shen Y, Matsuno Y, Fouse SD, Rao N, Root S, Xu R, Pellegrini M, Riggs AD, Fan G. X-inactivation in female human embryonic stem cells is in a nonrandom pattern and prone to epigenetic alterations. Proc. Natl. Acad. Sci. 2008; 105:4709–4714. [PubMed: 18339804]

Silva SS, Rowntree RK, Mekhoubad S, Lee JT. X-chromosome inactivation and epigenetic fluidity in human embryonic stem cells. Proc. Natl. Acad. Sci. 2008; 105:4820–4825. [PubMed: 18339803]

Smith ZD, Chan MM, Humm KC, Karnik R, Mekhoubad S, Regev A, Eggan K, Meissner A. DNA methylation dynamics of the human preimplantation embryo. Nature. 2014; 511:611–615. [PubMed: 25079558]

Takashima Y, Guo G, Loos R, Nichols J, Ficz G, Krueger F, Oxley D, Santos F, Clarke J, Mansfield W, et al. Resetting Transcription Factor Control Circuitry toward Ground-State Pluripotency in Human. Cell. 2014; 158:1254–1269. [PubMed: 25215486]

Tchieu J, Kuoy E, Chin MH, Trinh H, Patterson M, Sherman SP, Aimiuwu O, Lindgren A, Hakimian S, Zack JA, et al. Female Human iPSCs Retain an Inactive X Chromosome. Cell Stem Cell. 2010; 7:329–342. [PubMed: 20727844]

Theunissen TW, Powell BE, Wang H, Mitalipova M, Faddah DA, Reddy J, Fan ZP, Maetzel D, Ganz K, Shi L, et al. Systematic identification of culture conditions for induction and maintenance of naive human pluripotency. Cell Stem Cell. 2014; 15:471–487. [PubMed: 25090446]

Theunissen TW, Friedli M, He Y, Planet E, O'Neil RC, Markoulaki S, Pontis J, Wang H, Iouranova A, Imbeault M, et al. Molecular Criteria for Defining the Naive Human Pluripotent State. Cell Stem Cell. 2016

Vallot C, Ouimette J-F, Makhlouf M, Féraud O, Pontis J, Côme J, Martinat C, Bennaceur-Griscelli A, Lalande M, Rougeulle C. Erosion of X Chromosome Inactivation in Human Pluripotent Cells Initiates with XACT Coating and Depends on a Specific Heterochromatin Landscape. Cell Stem Cell. 2015; 16:533–546. [PubMed: 25921272]

Ware CB, Nelson AM, Mecham B, Hesson J, Zhou W, Jonlin EC, Jimenez-Caliani AJ, Deng X, Cavanaugh C, Cook S, et al. Derivation of naive human embryonic stem cells. Proc. Natl. Acad. Sci. 2014; 111:4484–4489. [PubMed: 24623855]

Yan L, Yang M, Guo H, Yang L, Wu J, Li R, Liu P, Lian Y, Zheng X, Yan J, et al. Single-cell RNA-Seq profiling of human preimplantation embryos and embryonic stem cells. Nat. Struct. Mol. Biol. 2013; 20:1131–1139. [PubMed: 23934149]
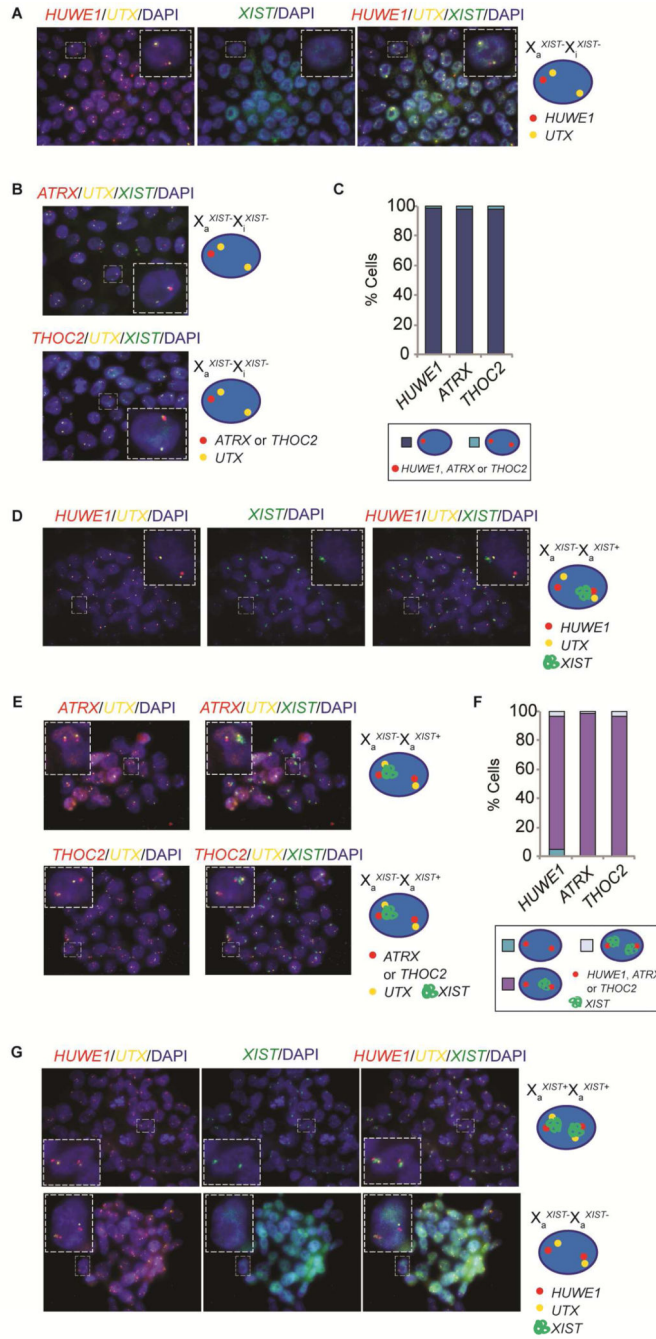
Figure 1. The X$_i$ of primed hESCs reactivates in the 5iLAF culture condition

(A) Representative RNA FISH images for primed UCLA1 at passage 16 (P16), detecting *XIST* and nascent transcription foci of *UTX*, (escapes XCI) and *HUWE1* (subject to XCI). Panels show *HUWE1* and *UTX* expression without *XIST* (left), *XIST* only (middle), and all three channels together (right) in DAPI-stained nuclei (blue). A nucleus with the most prevalent pattern is highlighted with a dotted box and enlarged, and its pattern depicted by the cartoon on the right.

(B) As in (A), but for the X-linked genes *ATRX* (top) or *THOC2* (bottom), showing only the merged panel with *XIST* and *UTX*.

(C) Quantification of the RNA FISH patterns for *XIST* and the X-linked genes *HUWE1, ATRX*, and *THOC2* in primed UCLA1 as shown in (A) and (B). Only cells with bi-allelic *UTX* expression were considered.

(D) Representative RNA FISH images of the most prominent X-chromosome state in naïve UCLA1 at P19 in 5iLAF media, detecting *HUWE1, XIST* and *UTX*, similar to (A).

(E) As in (D), but detecting the X-linked genes *ATRX* (top) or *THOC2* (bottom).

(F) Quantification of the RNA FISH patterns for *XIST* with *HUWE1, ATRX*, and *THOC2*, respectively, in naive UCLA1 as shown in (D) and (E) in cells with bi-allelic *UTX* expression.

(G) Representative RNA FISH images similar to (D), but for the bi-allelic *XIST* (top) and *XIST*-negative (bottom) X_aX_a patterns.
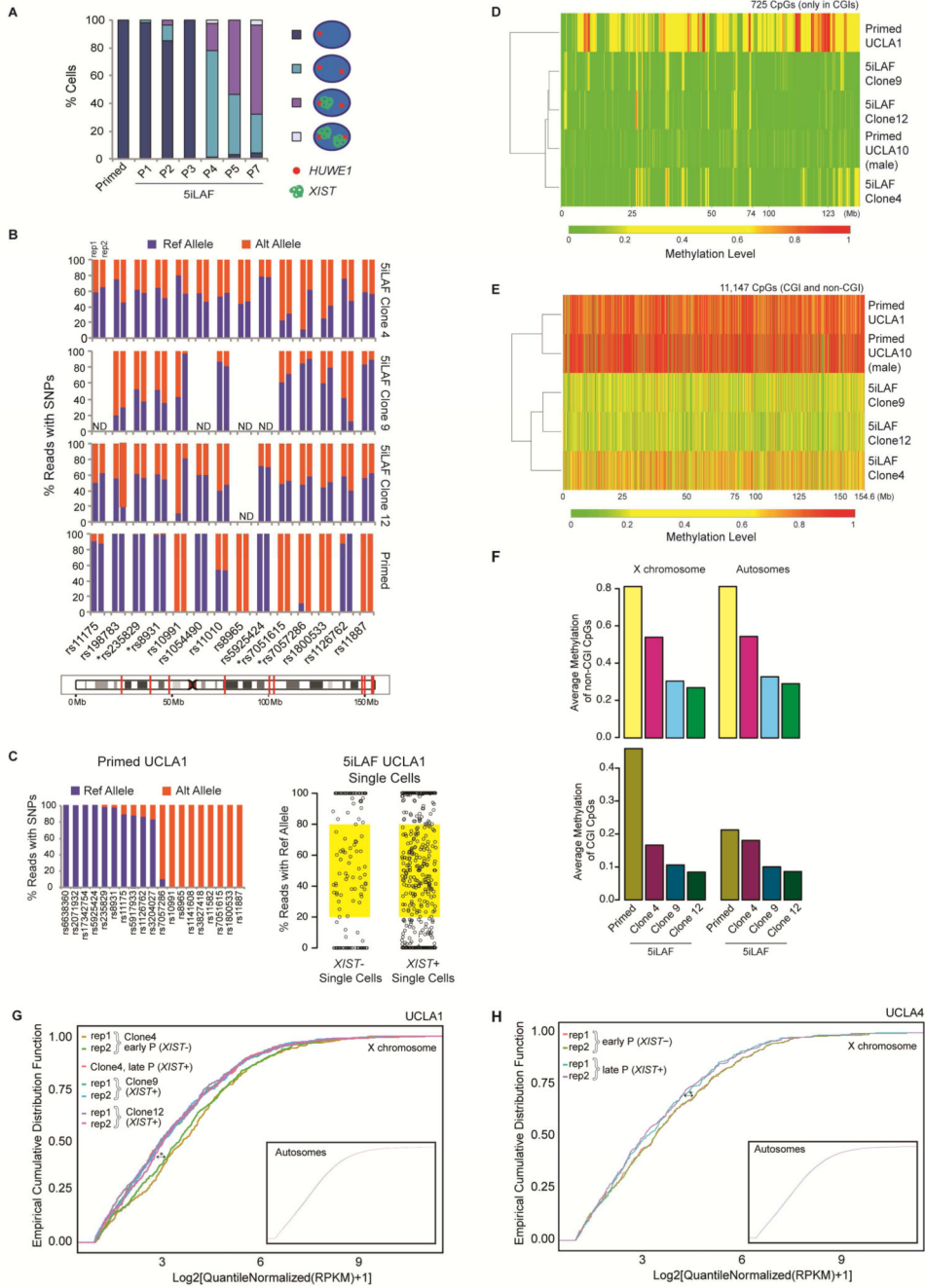
See also Figure S1.

Figure 2. X$_i$-reactivation leads to an *XIST* negative X$_a$X$_a$ intermediate before induction of *XIST* expression from the X$_a$

(A) Quantification of the RNA FISH patterns for *XIST* and *HUWE1* as UCLA1 progressed from the primed state at P12 to the naïve pluripotent state up to P7 in 5iLAF media. All counts were in naïve cells with two *UTX* foci.

(B) Allelic expression proportions of X-linked genes in the primed UCLA1 population, the naïve UCLA1 clone4 (at early passage, *XIST*-negative state), and the naïve *XIST*-positive UCLA1 clones 9 and 12, based on reads covering indicated SNPs, ordered along the X-

chromosome (depicted with red lines in the X-chromosome image below), in replicate RNA-seq data (rep1 and rep2, closely-spaced bars). SNPs located in the same gene were placed next to each other and marked with an asterisk (*). ND = Not Determined due to insufficient read coverage.

(C) Analysis of allelic expression proportions of X-linked genes in single *XIST*-negative and *XIST*-positive naïve UCLA1 cells. Single cells of naïve UCLA1 at early passage, when the population was still largely *XIST*-negative, and at later passage, when most cells were *XIST*-positive, were grouped into *XIST*-positive and *XIST*-negative cells based on their *XIST*-expression levels. The two graphs on the right show the allelic expression proportion of X-linked genes for each single cell with sufficient SNP coverage in these two groups, with each circle representing the proportion of one SNP in one single cell. Highlighted with yellow is the 20–80% range region where we considered X-linked gene expression from both X-chromosomes to take place. For comparison, the graph on the left plots the allelic ratio of the same SNPs used in the right in primed UCLA1 as described in (B).

(D) Heatmap of unsupervised hierarchical clustering of RRBS-based methylation levels of CpGs within X-linked CGIs. The number of CpGs considered is given. Mb (megabase) indicates the relative position on the X-chromosome.

(E) Heatmap as in (C), but for all X-linked CpGs covered by RRBS.

(F) Methylation averages of X-linked and autosomal CpGs outside (top) and within CGI's (bottom) in primed UCLA1 and the naïve clones 4 (*XIST*-negative), 9 and 12 (*XIST*-positive).

(G) Empirical cumulative distribution functions of X-linked gene expression for naïve UCLA1 clone4 at early (*XIST*-negative) and late (*XIST*-positive) passage, and the *XIST*-positive clones 9 and 12, based on replicate RNA-seq data sets where available (rep1, rep2). The inset shows autosomal expression data for the same samples in the same format. Asterisk (*) indicates statistically significant difference between the distributions of X-linked gene expression of both replicates of early passage (*XIST*-negative) clone4 compared to all other samples (p<0.0035 by Wilcoxon rank sum test with continuity correction). The X-linked and all autosomal distributions for all other samples were not significantly different from each other.

(H) Same as in (G), but for early (*XIST*-negative) and late (*XIST*-positive) passage naïve UCLA4 hESCs. X-linked but not autosomal gene expressions of both replicates of early passage (*XIST*-negative) samples were significantly different from replicate 2 (but not replicate 1) of late passage (*XIST*-positive) cells (p<0.05).

See also Figures S2 and S3.

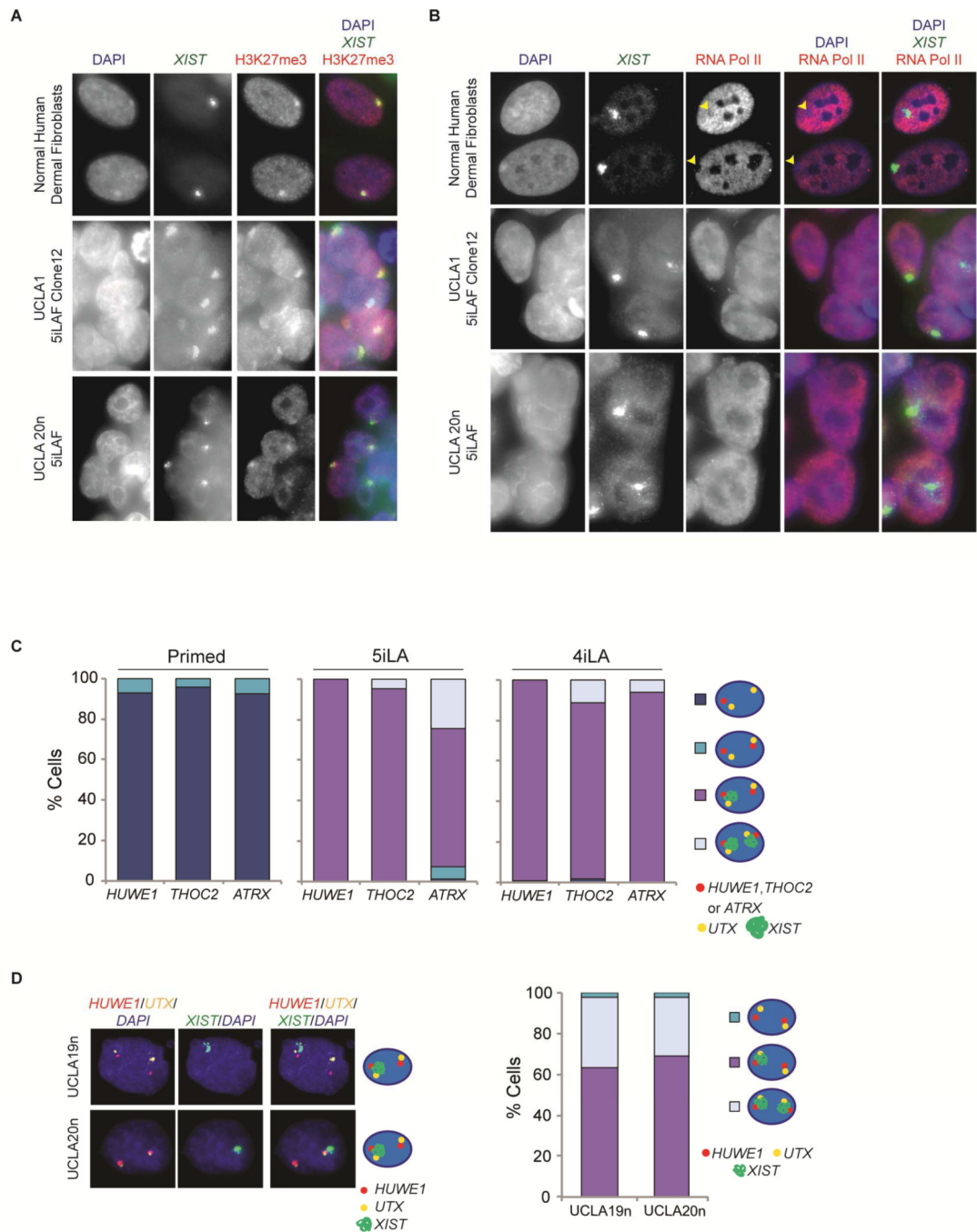**Figure 3. The *XIST* expressing X$_a$X$_a$ state is found in naïve hESC lines regardless of source**

(A) Immunofluorescence detection of H3K27me3 (red) combined with RNA FISH for *XIST* (green) in normal female fibroblasts (top), the naïve UCLA1 clone12 (middle), and blastocyst-derived naïve UCLA20n (bottom) cells.

(B) As in (A), except for RNA polymerase II (RNA PolII) and *XIST*. Yellow arrowheads demonstrate regions in nuclei devoid of RNA PolII signal under the *XIST* signal.

(C) Quantification of RNA FISH patterns of transcription foci of *HUWE1, ATRX*, and *THOC2*, respectively, and of *XIST* in primed, 5iLA- and 4iLA-cultured naïve WIBR3 hESCs.

(D) Representative RNA FISH images detecting *XIST, HUWE1*, and *UTX* in the blastocyst-derived naïve hESC lines UCLA19n and UCLA20n. RNA FISH patterns were stable throughout passaging and in the graph are quantified at P3 for both lines.
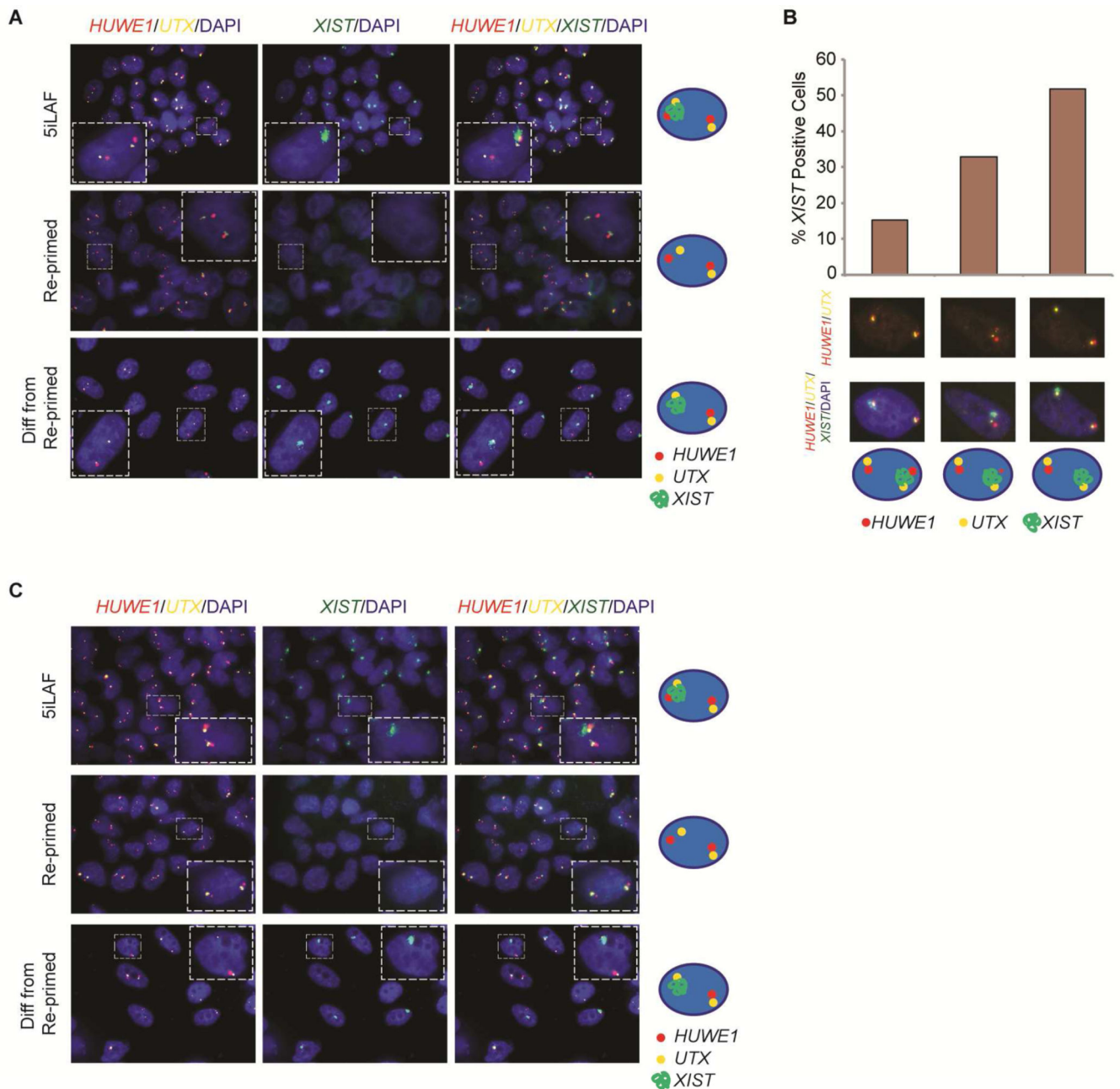
See also Figure S4.

Figure 4. Naïve hESCs initiate XCI upon differentiation

(A) Representative RNA FISH images for *XIST, HUWE1*, and *UTX* in naïve UCLA1 at P42 in 5iLAF, in the re-primed condition at P7, and after seven days of differentiation (Diff) from the re-primed state. A nucleus with the most prevalent pattern is highlighted with a dotted box and enlarged, and also depicted by the cartoon on the right.

(B) Quantification of *XIST*-expressing differentiated cells with different *HUWE1* transcription patterns (bi-allelic with equal transcription foci on both X-chromosomes, bi-allelic with a smaller transcription focus on the *XIST*-coated chromosome, and mono-allelic) in cells with bi-allelic *UTX* expression.

(C) Representative RNA FISH images as in (A), but for the naïve hESC line UCLA20n at P8 (naïve), P4 (re-primed), and after seven days of differentiation of re-primed state.
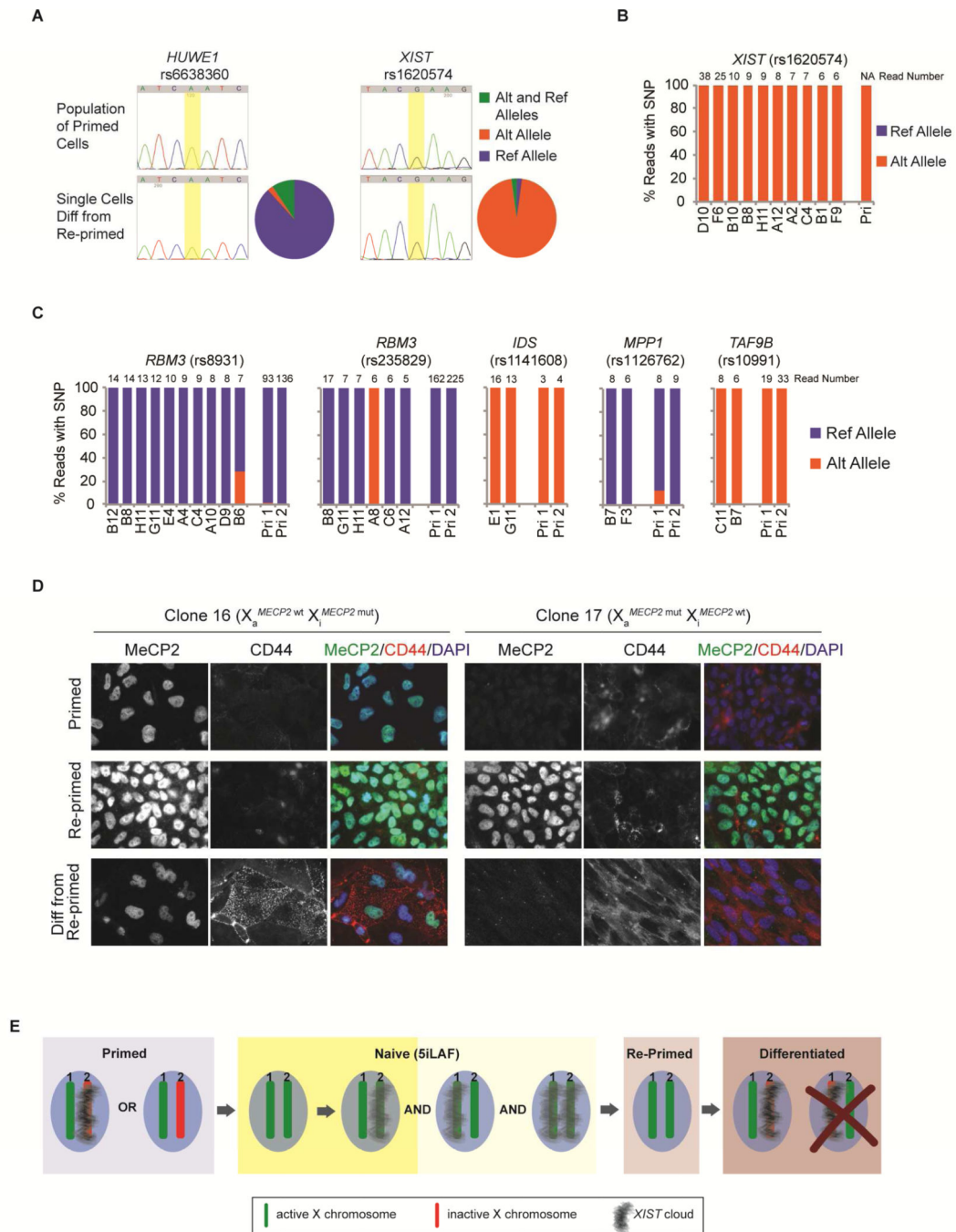
Figure 5. XCI in differentiating naïve cells is non-random

(**A**) Representative electropherograms from Sanger sequencing of SNP-containing regions in the *HUWE1* and *XIST* cDNA obtained from the primed UCLA1 population (at P19 for *HUWE1* and P4 for *XIST* analysis; top), and from an individual cell differentiated from the re-primed state after transition through the naïve state (bottom). Pie charts summarize the Sanger sequencing results for additional *XIST*-positive, single differentiated cells (43 individual cells for *HUWE1*, 47 for *XIST*), considering three expression categories: expression of only reference (Ref) allele, only alternate (Alt) allele, or both alleles.

(B) Allelic expression proportions of *XIST* based on RNA-seq reads (number of reads indicated on top) that covered the indicated SNP in single cells differentiated from naïve UCLA1 after transition through the re-primed state. The X-axis refer to single cell coordinates in a 96-well plate. For comparison, the allelic *XIST* proportion in primed UCLA1 was estimated from the Sanger sequencing electropherograms in (A, top).

(C) As in (B), but for the X-linked genes *RBM3* (two different SNPs), *IDS, MPP1, TAF9B*. Only *XIST*-expressing single cells were analyzed. Allelic expression proportions in primed UCLA1 were calculated from replicate RNA-seq data of the primed cell population (Pri1 and Pri2).

(D) Representative immunofluorescence images detecting MeCP2 and CD44 in hiPSC clones 16 and 17 harboring an X_a with wild type and mutant *MECP2*, respectively. Shown are primed hiPSCs (P17; top), re-primed cells (P3) after transition through the naïve 5iLAF for 3 passages (middle), and the day 7 differentiation product of the re-primed state (bottom).

(E) Schematic summary of X-chromosome dynamics as primed X_aX_i cells with or without *XIST* expression from the X_i transition to naïve pluripotency and differentiate.
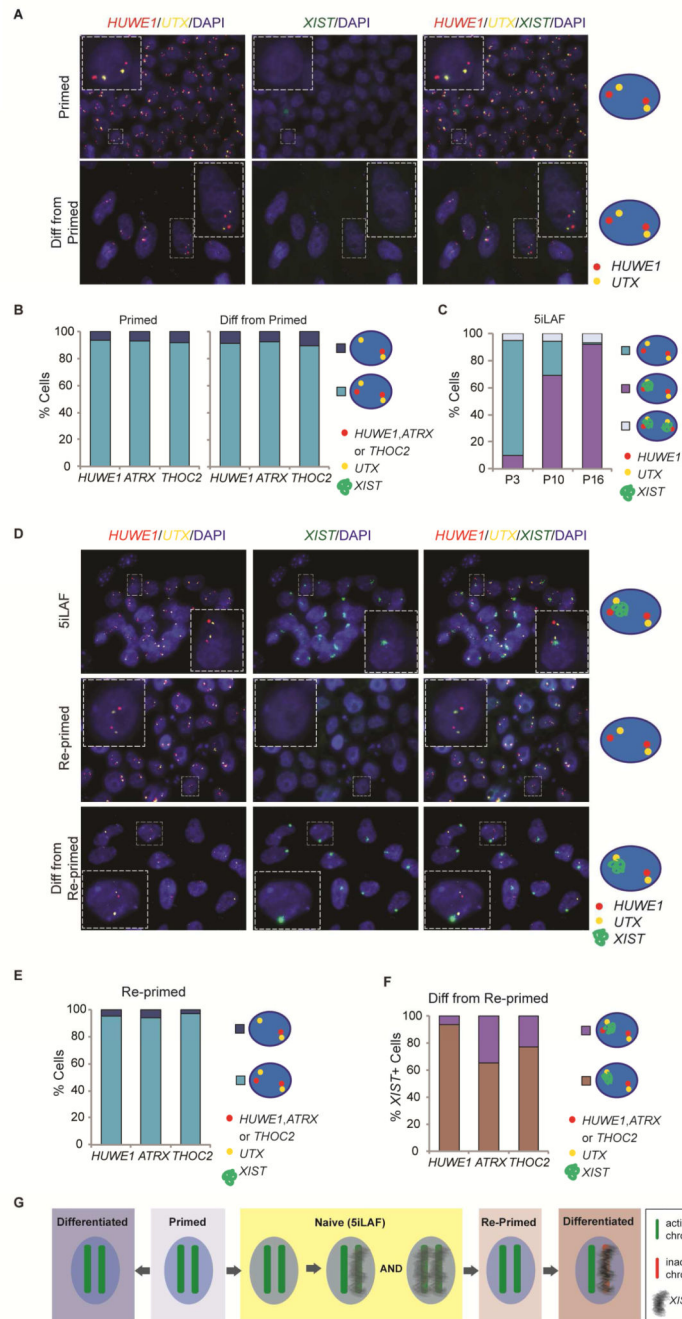
See also Figure S5.

Figure 6. Naïve pluripotency enables XCI in primed hESCs with an aberrant X_aX_a state

(A) Representative RNA FISH images detecting *XIST, HUWE1*, and *UTX* in primed UCLA9 (P15) and upon seven days of differentiation. A nucleus with the most prevalent pattern is highlighted with a dotted box and enlarged, and also depicted by the cartoon. **(B)** Quantification of RNA FISH patterns of *XIST* in combination with *HUWE1, ATRX*, and *THOC2*, respectively, in the primed state and its differentiated daughter cells. Only cells with biallelic *UTX* expression were quantified.

(C) Quantification of RNA FISH patterns of *XIST* and *HUWE1* in UCLA9 at indicated passages post 5iLAF conversion. Only cells with biallelic *UTX* expression were quantified.

(D) Representative RNA FISH images detecting *XIST, HUWE1,* and *UTX* in UCLA9 in the naïve state (P22), the re-primed state obtained by culturing naïve cells in the primed culture condition for 3 passages, and in day 7 differentiated cells derived from re-primed cells. In each row, a nucleus with the most prevalent pattern is highlighted with a dotted box and enlarged, and depicted by the cartoon on the right.

(E) As in (B), but for re-primed state.

(F) As in (B), but for differentiated UCLA9 described in (E).

(G) Schematic summary of the X-chromosome state of UCLA9 in indicated states.
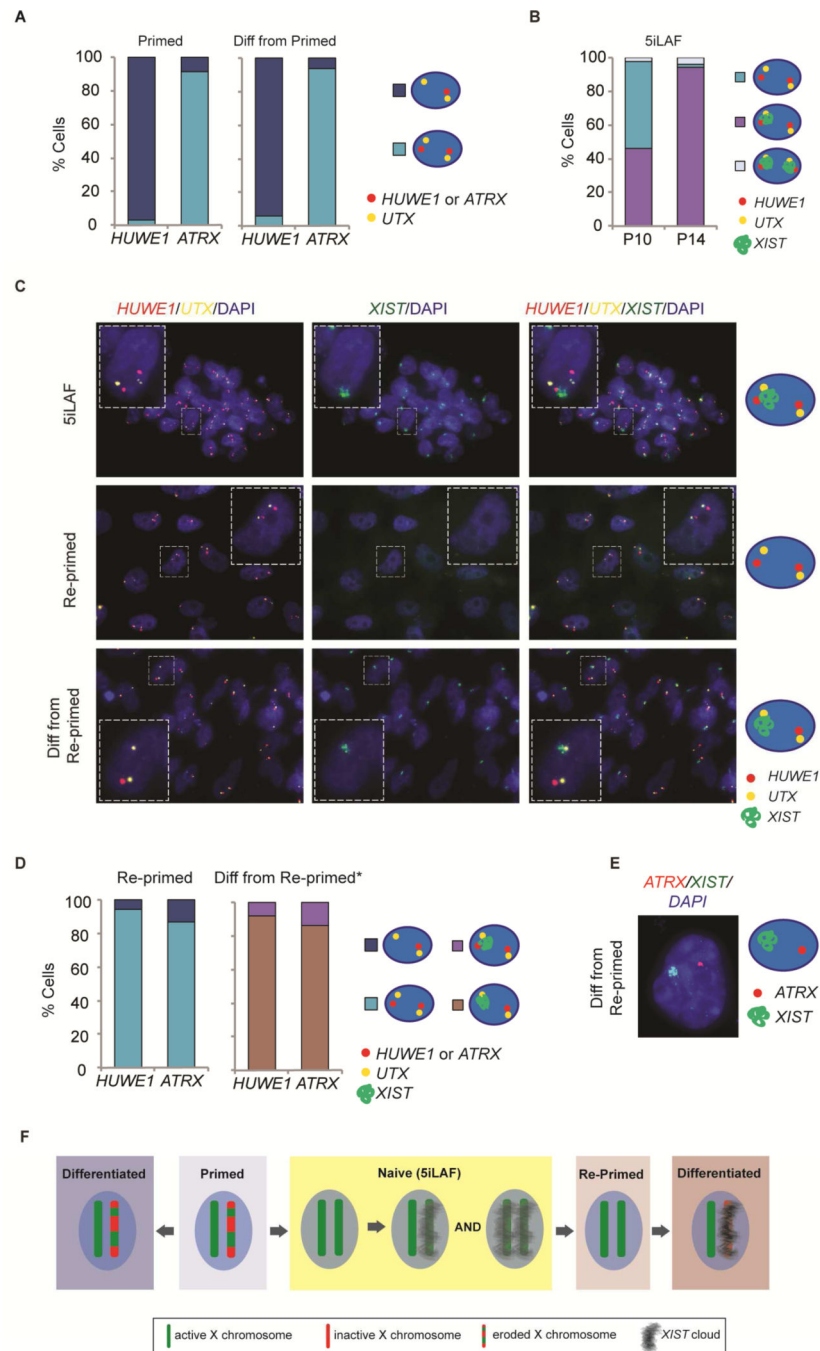
See also Figure S6.

Figure 7. Naïve pluripotency erases X$_i$-erosion of primed hESCs

(A) Quantification of RNA FISH patterns of *XIST* and *HUWE1*, or *XIST* and *ATRX* in primed UCLA4 and upon seven days of differentiation from the primed state. Only cells with bi-allelic *UTX* expression were quantified.

(B) Quantification of RNA FISH patterns of *XIST* and *HUWE1* in UCLA4 at indicated passages post 5iLAF conversion. Only cells with biallelic *UTX* expression were quantified.

(C) Representative RNA FISH images detecting *XIST, HUWE1*, and *UTX* in UCLA4 in the naïve state (P7), in the re-primed state obtained from the naïve state, and in day 7

differentiated cells derived from re-primed cells. A nucleus with the most prevalent pattern is highlighted with a dotted box and enlarged, and also depicted by the cartoon.

(D) Quantification of RNA FISH patterns in re-primed UCLA4 and their differentiated progeny in cells with bi-allelic *UTX* expression as in (A). Only *XIST*-expressing cells were considered in the differentiated state.

(E) Representative RNA FISH image detecting *XIST* RNA and nascent transcription foci of *ATRX* in differentiated cells originating from re-primed cells derived from naïve UCLA4.

(F) Schematic summary of the X-chromosome states of UCLA4 in indicated states.

See also Figure S7.